Differential-Series-Fed Dual-Polarized Traveling-Wave Array for Full-Duplex Applications

Zhang, Yiming; Li, Jia-Lin

Published in:
IEEE Transactions on Antennas and Propagation

DOI (link to publication from Publisher):
10.1109/TAP.2019.2948393

Publication date:
2020

Document Version
Accepted author manuscript, peer reviewed version

A Differential-Series-Fed Dual-Polarized Traveling-Wave Array for Full-Duplex Applications

Yi-Ming Zhang and Jia-Lin Li

***Abstract*—In this communication, an 8×8 dual-polarized traveling-wave antenna array is proposed and studied for in-band full-duplex applications. The proposed array consists of single-layer dual-polarized patch antennas with a simple feeding network. Despite the strong coupling among antenna elements, good suppression for the self-interference can be achieved by using differential feedings. To validate the study, an on-board prototype is developed, fabricated, and measured. Results show that good impedance matching responses are found, and high isolation of over 50 dB between the dual-polarized outputs is realized from less than 13.0 to 15.7 GHz. Meanwhile, small sidelobes and low cross-polarization levels with low insertion loss are observed, showing well-designed radiation responses.**

***Index Terms*—Self-interference, full-duplex, traveling wave, differential feeding, radiation efficiency.**

I. INTRODUCTION

Recently, studies on in-band full-duplex operations for wireless applications have attracted increasing interests, since the uplink and downlink are simultaneously operated under a single frequency carrier, resulting in a theoretically doubled spectrum efficiency compared with half-duplex schemes [1]-[3]. To realize a full-duplex system, one of the key challenges is the suppression of the strong self-interference that results from the limited isolation between the local transmitter (Tx) and receiver (Rx), where isolation of over 80 dB between the Tx and Rx ports is generally required. For antenna array-based systems, it is not possible to achieve such a high isolation by using only antenna-based self-interference suppression as a result of the complicated mutual coupling. Combining antenna-based, analog-based, and digital-based techniques is the necessary and primary method to achieve 80 dB or even higher isolations [4], [5]. For the analog-based suppression, it is usually based on the active circuit network. When an antenna-based passive suppression together with the cancellation of the digital domain could achieve the prescribed high isolation, the need of the analog-based cancellation network that is generally complex and power consuming can be avoided [6]. On the other hand, the digital-based suppression cannot suppress the self-interference when the receiver front-end is overloading, thus would prevent the recovery of the received signals [7]. Consequently, if a high self-interference suppression level could be achievable at the antenna level, full-duplex communications will be possible under low self-interference suppression levels for the subsequent digital-based cancellations.

This work was supported in part by the Natural Science Foundation of China (NSFC) (61601063). (*Corresponding author*: *Jia-Lin Li*)

The authors are with the School of Physics, University of Electronic Science and Technology of China, Chengdu 610054, China. (Email: ymzhang@std.uestc.edu.cn, jialinli@uestc.edu.cn.)

Yi-Ming Zhang is also with the Antenna, Propagation and Millimeter-wave Systems (APMS) Section, Aalborg University, Aalborg 9220, Denmark (e-mail: yiming@es.aau.dk).

Recently, studies on dual-polarized antennas for full-duplex systems are paid increasing attentions, since the isolation improvement can benefit from the polarization orthogonality [3], [4], [6], [8], [9]. From these studies, the system with simultaneous transmitting and receiving, where orthogonal polarizations are assigned for Tx and Rx, can be considered as a specified subset of the in-band full-duplex system. For single-antenna systems, high inter-port isolation can be achieved owing to the simple coupling by using dual-polarized antennas [8]. More recently, increasing efforts have been devoted to canceling/suppressing the self-interference in dual-polarized antenna arrays, especially large-scale arrays for high-gain applications, where complicated mutual coupling among antenna elements exists [3], [9]-[11]. In [9], a 4×4 differential-fed dual-polarized antenna array with high isolation of over 65 dB was reported, where the feeding network was complicated since 16 baluns were utilized. A dual-polarized 2×2 antenna array using multi-layer configuration was studied in [10]. The achieved isolation was approximately 35 dB by employing specified and complicated quasi-substrate integrated waveguide structure. Using additional decoupling techniques such as electromagnetic-bandgap structures can suppress the mutual coupling among antenna elements, which could simplify the feeding at the cost of bulky systems [12], [13]. On the other hand, using traveling-wave array configurations is an alternative to make the feeding networks simple and compact [14]-[17]. For instance, a dual-polarized traveling-wave linear antenna array with a simple series-fed network was studied in [14]. The simulated isolation between the two orthogonal ports in a single antenna element was over 30 dB but without measured results for the inter-port isolation of the linear array. In [15], a 6×2 dual-polarized antenna array with series-feeding was studied. Although differential feeding technique was utilized, a low isolation level of 18.6 dB was observed.

In this work, a Ku-band 8×8 dual-polarized antenna array featuring a high inter-port isolation level is discussed for in-band full-duplex applications, where orthogonal polarizations are assigned for Tx and Rx links respectively. The array consists of traveling-wave-based square patch elements with differential feeding networks that are realized by employing simple slotline-based baluns, leading to well-canceled self-interference resulting from the mutual coupling within the array. Moreover, lumped resistors are employed as loads to improve the impedance performance and radiation efficiency, making the proposed array working in a wide band and low insertion loss. The proposed array characterizes compactness, small sidelobes as well as high polarization purity. Both theoretical analyses and measurements are presented and good results are found.

II. DUAL-POLARIZED TRAVELING-WAVE ANTENNA ARRAY

Fig. 1 shows the configuration of the proposed Ku-band antenna array with improved inter-port isolation. The array consists of 4 subarrays and 16 identical resistors with resistance R. Each subarray is a 4×4 array composed of dual-polarized four-port square patch elements that are connected through the transmission lines with the characteristic impedance of Z_1. The patch elements are arranged with a center distance of $L = 0.59\lambda_0$ to provide identical excitation phase for

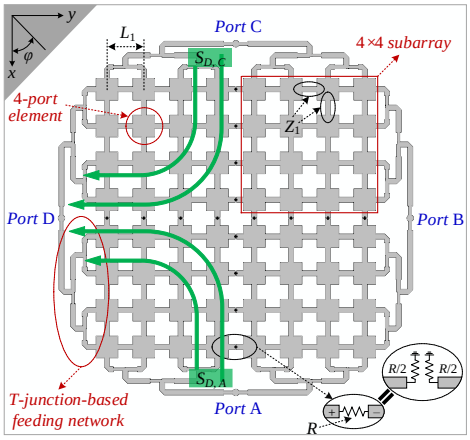

Fig.1. Configuration of the proposed dual-polarized antenna array. The array is of a single layer and printed on a substrate with the permittivity and thickness of 2.2 and 0.5 mm, respectively.

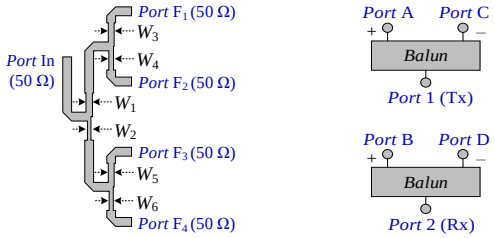

Fig.2. (a) Layout of the T-junction-based feeding network used in Fig. 1, where the optimal sizes are (unit: mm): W_1 = 1.1, W_2 = 0.6, W_3 = 1.0, W_4 = 0.8, W_5 = 1.05. W_6 = 0.7. (b) Feeding networks for ports A, B, C, and D.

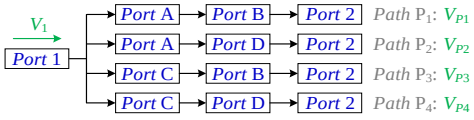

Fig. 3. Signal flow diagrams of the self-interference between ports 1 and 2.

all elements at the center frequency of 15.0 GHz. The isolation between the orthogonal ports within a single patch element is around 12 dB, leading to the strong self-interference. The size of the patch element is 6.9 mm×6.9 mm. The adjacent patch elements that belong to different subarrays are connected through the resistors under 50-Ω transmission lines. For each subarray, a T-junction-based feeding network is introduced as shown in Fig. 1 and Fig. 2(a). The feeding network is designed with unequal divisions, where the division ratios are 1:1.5:2:2.5 orderly corresponding to the ports F_1, F_2, F_3, and F_4. Thus, quasi-triangular amplitude distribution is provided for exciting each subarray. The radiation patterns of the array using such excitations could feature small sidelobes as discussed in [18]. Notice that the proposed configuration is still symmetrical despite the quasi-triangle distributions. Therefore, a four-port dual-polarized antenna array is obtained, where vertical polarization can be observed when both ports A and C are excited with the same magnitude but out of phase, and horizontal polarization can be obtained when ports B and D are excited under the same conditions. Hence, two baluns used in Fig. 2(b) are employed for differential feedings. Based on this, a two-port traveling-wave-based dual-polarized antenna array is realized.

Owing to the differential feedings, the resistors play the role of loads. For instance, when port 2 shown in Fig. 2(b) is excited, the voltages at two sides of the selected resistor depicted in Fig. 1 would be out-of-phase. Therefore, the resistor with the value of R can be decomposed as two resistors with the same value of $R/2$ in series and

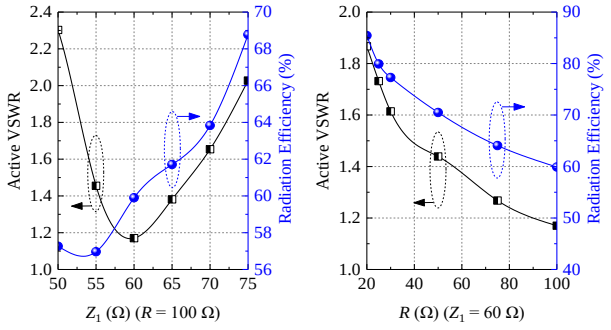

Fig. 4. Active VSWR of port A and radiation efficiency of the array with different values of (a) characteristic impedance Z_1 and (b) resistance R at 15.0 GHz, with ports A and C excited under same magnitude but out of phase.

further, they are terminated on the ground during the analysis. As a result, the value of the resistance is of great significance to improve the impedance matching, as discussed later. With the proposed architecture, the self-interference resulting from the mutual coupling between elements as well as the self-coupling within a single element can be well suppressed, leading to high isolation between ports 1 and 2 as discussed below.

Considering the reciprocity and without loss of generality, ports 1 and 2 are defined as Tx and Rx ports, respectively. The self-interference between Tx and Rx can be considered as combining four signal flow paths, as shown in Fig. 3. The input voltage at port 1 is defined as V_1 and the following discussions present the resulting complex voltage V_2 at the output interface of port 2, given by

$$\textit{Path}\ \mathrm{P}_1:\ V_{P1} = \left|S_{A,1}\right| e^{-j\varphi_1} \cdot S_{B,A} \cdot \left|S_{2,B}\right| e^{-j\varphi_1} \cdot V_1 \tag{1}$$

$$\textit{Path}\ \mathrm{P}_2:\ V_{P2} = \left|S_{A,1}\right| e^{-j\varphi_1} \cdot S_{D,A} \cdot \left|S_{2,D}\right| e^{-j\varphi_2} \cdot V_1 \tag{2}$$

$$\textit{Path}\ \mathrm{P}_3:\ V_{P3} = \left|S_{C,1}\right| e^{-j\varphi_2} \cdot S_{B,C} \cdot \left|S_{2,B}\right| e^{-j\varphi_1} \cdot V_1 \tag{3}$$

$$\textit{Path}\ \mathrm{P}_4:\ V_{P4} = \left|S_{C,1}\right| e^{-j\varphi_2} \cdot S_{D,C} \cdot \left|S_{2,D}\right| e^{-j\varphi_2} \cdot V_1 \tag{4}$$

$$\text{Total output at } \textit{Port}\ 2:\ V_2 = V_{P1} + V_{P2} + V_{P3} + V_{P4} \tag{5}$$

where the parameters S with different subscripts are the transmission coefficients among the related ports; φ_1 and φ_2 are the phases of the two outputs of the balun, respectively.

In view of the symmetry, it can be observed that

$$S_{B,A} = S_{B,C} = S_{D,A} = S_{D,C} \tag{6}$$

For ideal baluns, we have

$$\left|S_{A,1}\right| = \left|S_{C,1}\right| = \left|S_{B,2}\right| = \left|S_{D,2}\right|, \quad \varphi_1 = \varphi_2 + \pi \tag{7}$$

Based on (1)-(7), it can be seen that the voltage V_2 is zero, resulting in good cancellations for self-interference by using the proposed architecture. Moreover, the proposed array scheme is compact with simple feeding networks and low cost, making it attractive for antenna array-based full-duplex applications.

III. Performance Analysis of the Proposed Array

In this section, full-wave simulations and graphical studies of the two parameters Z_1 and R are performed to investigate and improve the 8×8 array performance, where ports A and C are simultaneously excited with the same magnitude but out of phase. Figs. 4(a) and 4(b) illustrate the active VSWR of port A and the radiation efficiency of the array against Z_1 and R at 15.0 GHz, respectively. It is observed that the active VSWR are over 2.2, indicating poor impedance matching when the values of Z_1 and R are of the original settings of 50 Ω and 100 Ω, respectively. This is mainly because of the small distance between the adjacent elements, leading to strong mutual coupling and thus

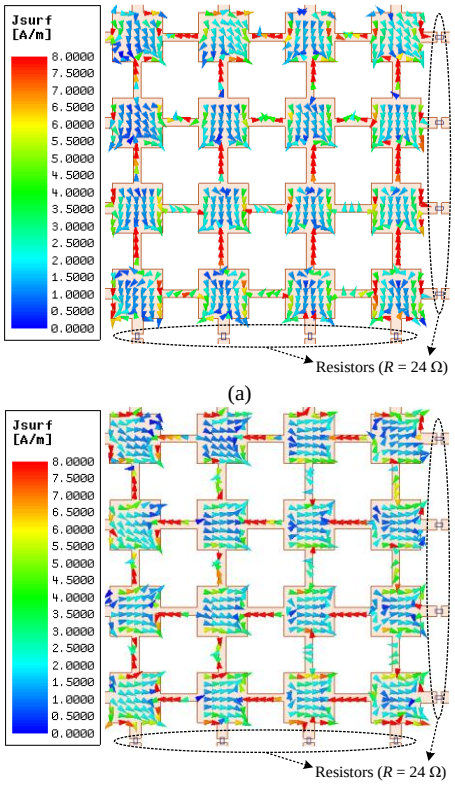

Fig. 5. Current distributions of the 4×4 subarray at the upper-left corner of the 8×8 array. (a) Ports A and C are excited under the same magnitude but out of phase. (b) Ports B and D are excited under the same magnitude but out of phase.

degrading the impedance matching of the array. Meanwhile, the radiation efficiency is approximately 58% as a result of the power dissipations among the loaded resistors.

On the other hand, it is seen from Fig. 4(a) that by optimally determining the value of Z_1, good impedance matching can be obtained. For instance, the active VSWR is below 1.2 when $Z_1 = 60\ \Omega$, with the radiation efficiency of approximately 60%. Despite that the improvements of impedance matching are observed under some values of Z_1, the achieved efficiencies are still relatively low. Seeing that the power is partially delivered to the resistors, the impact of the values of R is further studied as recorded in Fig. 4(b) with $Z_1 = 60\ \Omega$. It is found that a smaller resistance value results in a higher radiation efficiency but suffering from a worse impedance matching. This indicates that the selection for the resistance is a tradeoff between the impedance matching and the radiation efficiency. Notice that in spite of the different values of Z_1 and R, the self-interference cancellation could not be affected due to the symmetry. Therefore, the design of the array can be simplified as two steps: (1) determining the value of Z_1 to improve the transmission response of the single 4×4 subarray; (2) optimizing the resistor R to get a high radiation efficiency for the 8×8 array under a determined Z_1. Based on the above discussions, the optimized values of $Z_1 = 60\ \Omega$ and $R = 24\ \Omega$ are selected.

Fig. 5 illustrates the full-wave simulated results of the surface current distributions of the 4×4 subarray at the upper-left corner of the 8×8 array, with the selected values of Z_1 and R. The results indicate that vertical polarization is generated when ports A and C are excited with out of phase, and horizontal polarization is obtained when ports B and D are excited under the out of phase. This is consistent with the discussions provided in Section II. Owing to the symmetry, similar results can be observed for the other three subarrays, which are not

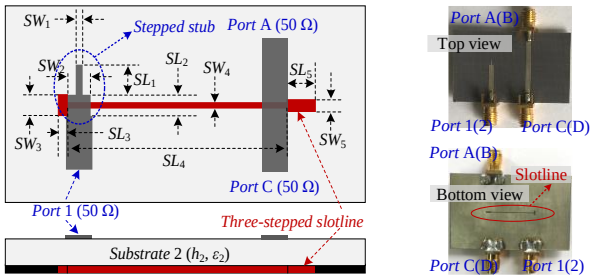

Fig. 6. (a) Configuration of the proposed balun. (b) Photos of the balun.

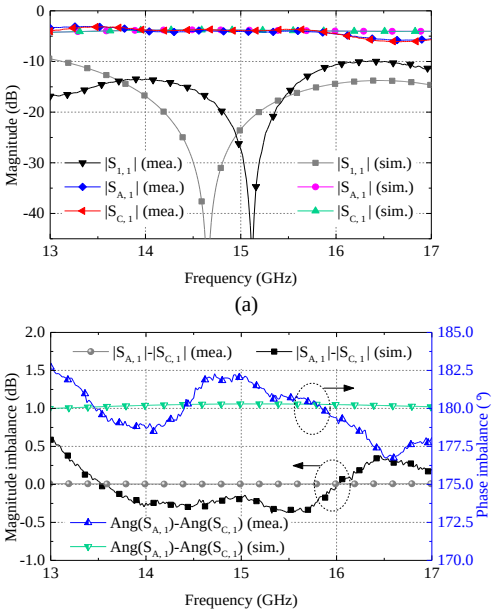

Fig. 7. Measured and simulated transmission responses of the developed balun. (a) S parameters. (b) Magnitude and phase imbalances.

detailed for brevity.

The above discussions verify the self-interference suppressions of the proposed scheme and investigate the influence of parameters Z_1 and R on the impedance matching as well as the radiation performance. Next, the practical implementation of the array is discussed.

IV. Ku-Band Slotline-Based Balun

As illustrated in Fig. 2, two baluns are employed for differential-feeding purposes. Here, a simple and wideband slotline-based balun for C-band applications presented in [9] is introduced. In order to realize a Ku-band balun, the structure is further evolved compared with the one in [9]. As described in Fig. 6(a), the improved balun consists of a slotline and two transmission lines crossing the slotline. The slotline is composed of three stepped slots. For the input port, an open-ended stepped stub is loaded at the end of a 50-Ω transmission line for impedance matching. It can be seen that the phase difference between the two outputs would be 180 °within a wide bandwidth. On account of the transmission line theory, good matching performance can be obtained by synthesizing the characteristic impedances and the electric lengths of the stepped stub and the slotline, thus not detailed here for brevity. Notice that the physical size of SL_4 based on the calculated electrical length θ_4 might be less than the width of the 50-Ω transmission lines, which would lead to strong mutual couplings between the transmission lines and further affect the impedance matchings. Consequently, the realized length of SL_4 is referred to the electric length of (θ_4+360˚), providing enough

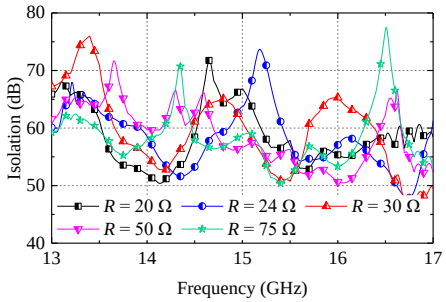

Fig. 8. Full-wave simulated isolation performance of the 8×8 array integrated with the proposed baluns against different values of *R*.

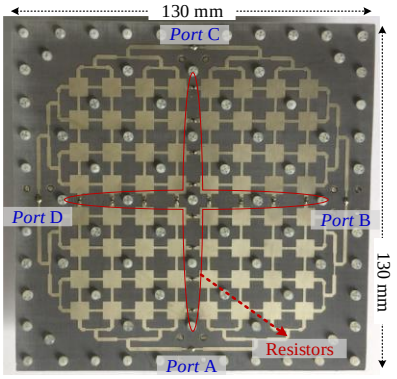

Fig. 9. Photographs of the developed 8×8 antenna array.

separation of the two transmission lines but maintaining the performance.

For the array prototype, two Ku-band slotline-based baluns centered at 15.0 GHz are designed, fabricated and measured, as shown in Fig. 6(b). The optimal dimensions are (unit: mm): SL_1 = 2.2, SL_2 = 1.6, SL_3 = 0.6, SL_4 = 17.9, SL_5 = 2.1, SW_1 = 0.3, SW_2 = 1.8, SW_3 =1.6, SW_4 =0.2, SW_5 = 0.5. The thickness and the relative permittivity of the substrate are 1.0 mm and 2.65, respectively. Fig. 7 describes the measured transmission responses of the proposed balun. The achieved impedance bandwidth is from less than 13.0 to over 17.0 GHz referring to $|S_{1,1}| \leq -10$ dB with an insertion loss of around 0.8 dB. The measured magnitude and phase imbalances are within ±0.5 dB and ±3.5 ºrespectively, exhibiting the well-designed electric performance.

To further investigate the implication of the value *R* on the isolation performance of the proposed 8×8 array, full-wave simulations of the array integrated with the proposed baluns are carried out. The results are illustrated in Fig. 8. It is seen that the isolation levels are better than 50 dB in almost the entirely studied frequency band against different values of *R*. This denotes that the value of *R* has nearly no effect on the isolation response of the proposed array, as expected. Next, an on-board prototype of the array is developed and built for demonstration purposes. The simulated results are provided along with the measurements.

V. Measurements of the Developed Demonstrator

The developed demonstrator based on the proposed architecture is fabricated and assembled, as pictured in Fig. 9, where a metal jig and some plastic screws are used for supporting and fixing purposes. The overall size of the array is 130 mm × 130 mm.

The 8×8 antenna array and the two baluns are connected by cables to measure the overall performance. The measured impedance matching and isolation responses of the antenna array integrated with the two baluns are illustrated in Fig. 10. As discussed in Section II, the design procedure of the array is operated based on the impedance matching and radiation performance at the center frequency of 15.0 GHz. Therefore, the impedance matching between the four-port antenna array shown in Fig. 1(a) and the proposed baluns would be degraded when the operation frequency offsets from 15.0 GHz. Despite this mismatching, the developed antenna array could also characterize a wide impedance matching bandwidth, ranging from

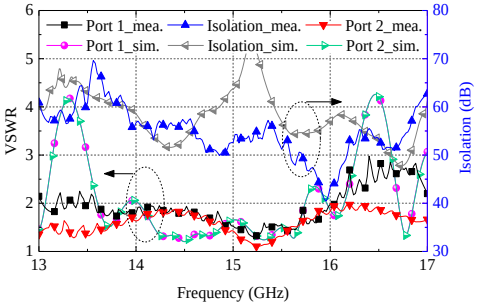

Fig. 10. Impedance matching and isolation responses of the demonstrator.

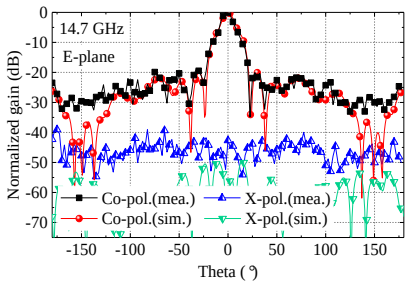

(a)

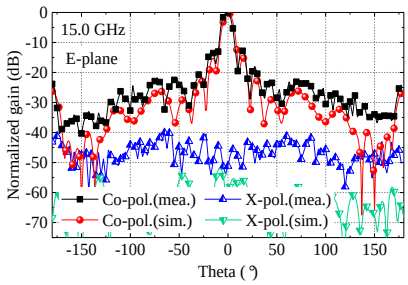

(b)

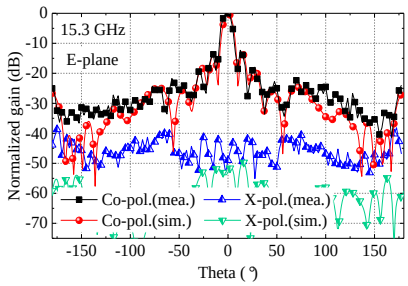

(c)

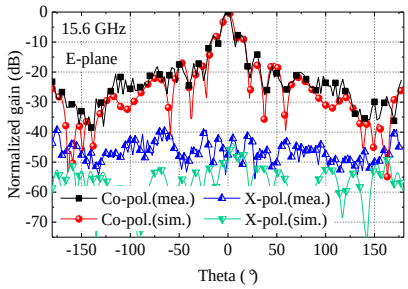

(d)

Fig. 11. Radiation patterns at E-plane when port 1 is excited. (a) 14.7 GHz. (b) 15.0 GHz. (c) 15.3 GHz. (d) 15.6 GHz.

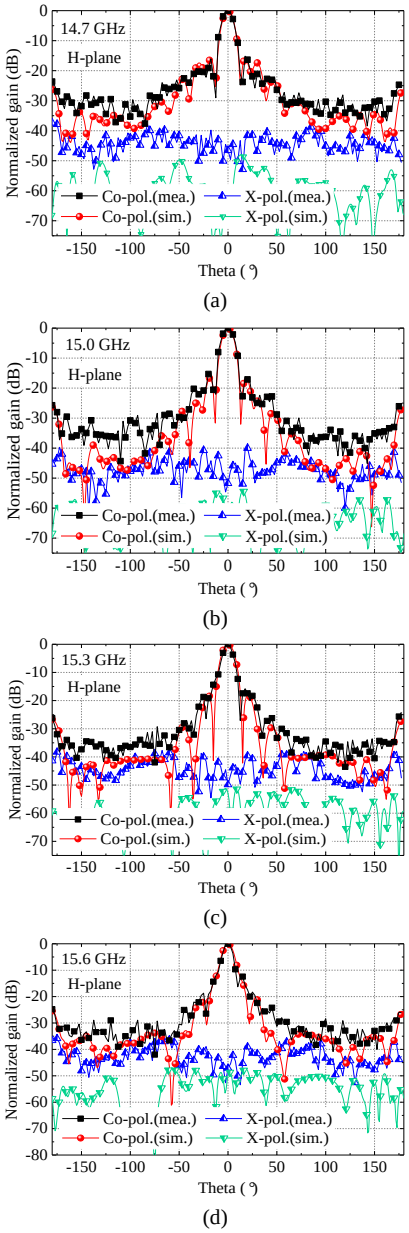

Fig. 12. Radiation patterns at H-plane when port 1 is excited. (a) 14.7 GHz. (b) 15.0 GHz. (c) 15.3 GHz. (d) 15.6 GHz.

13.6 to 16.0 GHz. Moreover, a high isolation level of over 50 dB is realized from 13.6 to 15.7 GHz, exhibiting the well-designed self-interference suppression. The measured isolation exhibits some degradations (less than 50 dB) near 16.0 GHz. This is mainly due to the magnitude and phase imbalances resulting from the fabrication and assembling errors in practice.

Figs. 11 and 12 record the radiation patterns at 14.7 GHz, 15.0 GHz, 15.3 GHz, and 15.6 GHz, respectively, when port 1 is excited. It is seen that good consistency between the measured and simulated results is observed. On both E-plane and H-plane, the 3-dB beamwidths are approximately 10 °and low cross-polarization levels of below –40 dB are observed. Owing to the symmetry, the results when port 2 is excited are similar to those when port 1 excited, thus not provided here for brevity. The measured maximum gains are illustrated in Fig. 13. Measurements indicate that with a maximum gain of 22.4 dBi, the achieved 3-dB gain bandwidth is from 14.5 to 15.9 GHz for either port 1 or port 2 as the excitation. The full-wave

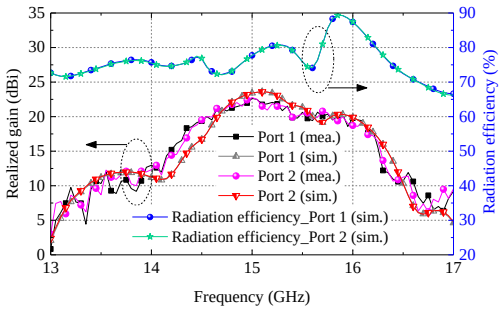

Fig. 13. Realized gain and radiation efficiency.

simulated radiation efficiencies are also recorded in Fig. 13, where one can see a high efficiency of over 72% is found within most of the studied frequency band. The simulated result shown in Fig. 4 at 15.0 GHz is 83% with the selected R = 24 Ω under the condition of ideal excitation (without insertion loss for ports A and C). For the results plotted in Fig. 13, the simulated radiation efficiency of 77% at 15.0 GHz is found when the array is integrated with the proposed baluns. Owing to small insertion losses of the baluns, the results shown in Fig. 13 are slightly degraded at 15.0 GHz. It is noted that the simulated radiation efficiency is 90% near 15.8 GHz. This might be due to the transmission response between adjacent patch elements being changed when the operation frequency offsets from the center frequency of 15.0 GHz. Consequently, the radiation efficiency might be enhanced but suffering from the degradation of the impedance matching as discussed in Section II and described in Fig. 10 where the simulated VSWR is over 2.0 around 15.8 GHz. Despite no measurements as a result of the lack of 3D-test environment in our laboratory currently, good agreement between simulations and measurements for the radiation pattern and realized gain could make us reasonably estimating the radiation efficiency from simulations. In general, these results indicate the self-interference resulting from the mutual coupling within the array is well-suppressed, while maintaining the radiation performance with small sidelobes and low cross-polarization levels.

For performance comparisons, some recently published dual-polarized antennas using several isolation-improvement methods are listed in Table I. It is seen from [10] and [19] that by using Q-SIW- and SIRMHs-based schemes, the enhancement levels of the isolation are 14 dB and 17 dB respectively compared to the original dual-polarized antennas, at the cost of complicated configurations. Besides, the two schemes are effective for a 2 ×2 array or a single patch element, but not suitable for large-scale arrays. The scheme presented in [3] features a high improvement level (over 27 dB) of the isolation, but only suitable for linear arrays. For the proposed 8 ×8 dual-polarized antenna array, a simple differential-series-fed configuration is utilized, leading to a high isolation level of over 50 dB within a wide frequency band. Referring to the isolation level (around 12 dB) between the orthogonal ports for a single four-port patch element mentioned in Fig. 1, significant improvement of over 38 dB for the studied 8 ×8 array is achieved. It is believed the enhancement of the isolation could definitely release the burden of the later stages including the digital-based suppressions. Moreover, the proposed 8 ×8 dual-polarized array characterizes simple and compact architecture, and further, it can be readily extended to large-scale arrays. The future research related to this work will be dedicated to the practical implementation of the full-duplex systems based on the proposed antenna array. To improve and verify the practical feasibility, further investigations associated with the digital-based self-interference cancellation method as well as the system capacity analysis are of importance.

TABLE I
PERFORMANCE COMPARISONS AMONG SOME PUBLISHED DUAL-POLARIZED ANTENNAS AND THE PROPOSED ANTENNA ARRAY

Ref./Year	[3]/2019	[10]/2018	[19]/2014	**This work**
Antenna type	1×4 Patch array	2×2 Patch array	Single patch	8×8 Patch array
Element center distance	$0.5\lambda_0$ @5.0 GHz	$0.66\lambda_0$ @13.8 GHz	–	$0.59\lambda_0$ @15.0 GHz
Matching bandwidth (GHz)	4.75~5.18 (8.6%)	11.9~15.4 (26.4%)	11.5~15.3 (28.4%)	13.6~16.0 (16.2%)
Complicated configuration	No	Yes	Yes	No
Improvement method of the isolation	Differential feeding	Q-SIW [a]	SIRMHs [b]	Differential feeding
Improvement level of the isolation	27 dB	14 dB	17 dB	38 dB
Isolation bandwidth [c] (GHz)	4.75~5.18 (≥ 50 dB) 8.6%	11.9~14.8 (≥ 40 dB) 21.7%	11.5~15.3 (≥ 40 dB) (28.4%)	13.6~15.7 (≥ 50 dB) 14.3%
Peak gain (dBi)	12.3	–	8.6	22.4
Radiation efficiency	> 80%	–	–	> 72% [d]
3-dB gain bandwidth [d] (GHz)	4.75~5.18 (8.6%)	–	11.5~15.3 (28.4%)	14.5~15.9 (9.2%)

[a] denotes the quasi-substrate integrated waveguide.
[b] denotes the substrate-integrated rows of metalized via holes.
[c] denotes the measured results in the matched frequency band.
[d] denotes the full-wave simulated results in the isolation frequency band.

VI. CONCLUSION

In this work, a Ku-band dual-polarized traveling-wave array with a differential-fed architecture for isolation enhancement is proposed and studied for full-duplex applications. By loading lumped resistors, the radiation and the impedance matching performance are improved effectively. The full-wave based analysis verifies the self-interference resulting from the mutual coupling among the antenna array elements can be well canceled, thus exhibiting good inter-port isolation response. Besides, the influence of the loaded resistors on the isolation is negligible due to the symmetry. For demonstration purposes, an on-board prototype is developed and examined experimentally. By incorporating with the proposed slotline-based balun, a high isolation level of over 50 dB is realized. Moreover, the proposed scheme is compact with simple feeding networks, making it attractive for large-scale dual-polarized array-based systems.

REFERENCES

[1] A. H. Abdelrahman and D. S. Filipovic, "Antenna system for full-duplex operation of handheld radios," *IEEE Trans. Antennas Propag.*, vol. 67, no. 1, pp. 522-530, Jan. 2019.

[2] F. Chen, R. Morawski, and T. Le-Ngoc, "Self-interference channel characterization for wideband 2×2 MIMO full-duplex transceivers using dual-polarized antennas," *IEEE Trans. Antennas Propag.*, vol. 66, no. 4, pp. 1967-1976, Apr. 2018.

[3] Y.-M. Zhang, S. Zhang, J.-L. Li, and G. F. Pedersen, "A dual-polarized linear antenna array with improved isolation using a slotline-based 180° hybrid for full-duplex applications," *IEEE Antennas Wireless Propag. Lett.*, vol. 18, no. 2, pp. 348-352, Feb. 2019.

[4] J. Zhou, N. Reiskarimian, J. Diakonikolas, T. Dinc, T. Chen, G. Zussman, and H. Krishnaswamy, "Integrated full duplex radios," *IEEE Commun. Mag.*, vol. 55, no. 4, pp. 142-151, Apr. 2017.

[5] B. Debaillie, D.-J. V. D. Broek, C. Lavín, B. V. Liempd, E. A. M. Klumperink, C. Palacios, J. Craninckx, B. Nauta, and A. Pärssinen, "Analog/RF solutions enabling compact full-duplex radios," *IEEE J. Sel. Areas Commun.*, vol. 32, no. 9, pp. 1662–1673, Sep. 2014.

[6] D. Korpi, M. Heino, C. Icheln, and K. Haneda, " Compact Inband Full-Duplex Relays With Beyond 100 dB Self-Interference Suppression: Enabling Techniques and Field Measurements," *IEEE Trans. Antennas Propag.*, vol. 65, no. 2, pp. 960–965, Feb. 2017.

[7] L. Laughlin, M. A. Beach, K. A. Morris, and J. L. Haine, "Optimum single antenna full duplex using hybrid junctions," *IEEE J. Sel. Areas Commun.*, vol. 32, no. 9, pp. 1653-1661, Sep. 2014.

[8] H. Nawaz, and I. Tekin, "Dual-polarized, differential fed microstrip patch antennas with very high interport isolation for full-duplex communication," *IEEE Trans. Antennas Propag.*, vol. 65, no. 12, pp. 7355-7360, Dec. 2017.

[9] Y.-M. Zhang and J.-L. Li, "A dual-polarized antenna array with enhanced interport isolation for far-field wireless data and power transfer," *IEEE Trans. Veh. Technol.*, vol. 67, no. 11, pp. 10258-10267, Nov. 2018.

[10] W. Wang, J. Wang, A. Liu, and Y. Tian, "A novel broadband and high-isolation dual-polarized microstrip antenna array based on quasi-substrate integrated waveguide technology," *IEEE Trans. Antennas Propag.*, vol. 66, no. 2, pp. 951-956, Feb. 2018.

[11] M. A. Islam and N. C. Karmakar, "A 4×4 dual polarized mm-wave ACMPA array for a universal mm-wave chipless RFID tag reader," *IEEE Trans. Antennas Propag.*, vol. 63, no. 4, pp. 1633-1640, Apr. 2015.

[12] J.-Y. Lee, S.-H. Kim, and J.-H. Jang, "Reduction of mutual coupling in planar multiple antenna by using 1-D EBG and SRR structures," *IEEE Trans. Antennas Propag.*, vol. 63, no. 9, pp. 4194-4198, Sep. 2015.

[13] L. Yang, M. Fan, F. Chen, J. She, and Z. Feng, "A novel compact electromagnetic-bandgap structure and its applications for microwave circuits," *IEEE Trans. Microw. Theory Tech.*, vol. 53, no. 1, pp. 183-190, Jan. 2005.

[14] A. Vallecchi and G. B. Gentili, "Design of dual-polarized series-fed microstrip arrays with low losses and high polarization purity," *IEEE Trans. Antennas Propag.*, vol. 53, no. 5, pp. 1791-1798, May 2005.

[15] R. D. Bari, T. Brown, S. Gao, M. Notter, D. Hall, and C. Underwood, "Dual-polarized printed S-band radar array antenna for spacecraft applications," *IEEE Antennas Wireless Propag. Lett.*, vol. 10, pp. 987-990, 2011.

[16] Y. Hirayama, K. Sakakibara, H. Umemura, K. Miyazaki, and N. Kikuma, "Effect of wall-surrounded slot on stepped narrow wall for bandwidth enhancement of partially parallel-feeding waveguide traveling-wave array," *IEEE Trans. Antennas Propag.*, vol. 65, no. 8, pp. 3976-3985, Aug. 2017.

[17] V. Ravindra, P. R. Akbar, M. Zhang, J. Hirokawa, H. Saito, and A. Oyama, "A dual-polarization X-band traveling-wave antenna panel for small-satellite synthetic aperture radar," *IEEE Trans. Antennas Propag.*, vol. 65, no. 5, pp. 2144-2156, May 2017.

[18] J. D. Kraus and R. J. Marhefka, "Chapter 11: Arrays of dipole and of apertures," in *Antennas*, 2nd. McGraw-Hill, U.S., 2012, pp. 517-520.

[19] S.-J. Li, J. Gao, X. Cao, Z. Zhang, and D. Zhang, "Broadband and high-isolation dual-polarized microstrip antenna with low radar cross section," *IEEE Antennas Wireless Propag. Lett.*, vol. 13, pp. 1413-1416, Feb. 2014.